Soil Science
and Environment

ARTICLE

Open Access

https://doi.org/10.48130/sse-0024-0001
Soil Science and Environment **2024**, 3: e001

Effect and model analysis of iron-modified biochar on chloridion and cadmium ion transport in loessial soil

Chengfeng Ma[1,2], Yiru Bai[2,3], Cheng Yuan[1,2], Yan Ma[2,3] and Youqi Wang[1,2*]

[1] *School of Ecology and Environment, Ningxia University, Yinchuan 750021, China*
[2] *Breeding Base for State Key Laboratory of Land Degradation and Ecological Restoration in Northwestern China, Ningxia University, Yinchuan 750021, China*
[3] *School of Geography and Planning, Ningxia University, Yinchuan 750021, China*
* Corresponding author, E-mail: wyq0563@163.com

Abstract

Iron-modified biochar is an environmently-friendly soil amendment, which plays an important role in regulating heavy metal transport in loessial soil. In this study, the mass ratio of iron-modified biochar to loessial soil was set to 0%, 1%, 2%, 3%, 4%, and 5% as CK, T1, T2, T3, T4, and T5 treatments, respectively. Based on solute transport experiments, the transport process of chloridion (Cl^-) and cadmium ion (Cd^{2+}) in soil adding iron-modified biochar was fitted using the convection-dispersion equation (CDE) and two-zone model (TRM). The results showed that the saturated hydraulic conductivity (*Ks*) gradually decreased to 93.70%, 84.13%, 83.33%, 79.60%, and 66.67% compared with CK, with increased iron-modified biochar addition amount. The total duration time of the equilibrium ion concentration was increased from 1.79 to 40.81 h, indicating that the initial and complete transport time of heavy metals was significantly retarded with the increase of iron-modified biochar addition amount. The mean intervoid water velocity (*v*) obtained from model fitting was opposite to the trend of the amount of iron-modified biochar. The fitting data of the CDE equation and TRM model were in good agreement with the experimental data, whereas the better simulation accuracy of the TRM model was observed according to the higher correlation coefficient ($R^2 > 0.99$) and lower root mean square error (*RMSE*) than the CDE equation. These findings indicate that iron-modified biochar effectively retards the transport of heavy metal ions in soil, which could provide a theoretical basis and technical ideas for the remediation of heavy metal-contaminated soil.

Citation: Ma C, Bai Y, Yuan C, Ma Y, Wang Y. 2024. Effect and model analysis of iron-modified biochar on chloridion and cadmium ion transport in loessial soil. *Soil Science and Environment* 3: e001 https://doi.org/10.48130/sse-0024-0001

Introduction

As one of the important components of the ecosystem, soil is not only the most basic carrier in agricultural production but also the ultimate destination of environmental pollutants (Zhang et al., 2020a; Gil et al., 2018). In recent years, various heavy metals have entered soil through different processes (e.g., industry, agriculture, transportation, and other ways) with the rapid development of the social economy, which exhibits a significant impact on human health and ecological security (Muhammad et al., 2021). According to the National Soil Pollution Survey Bulletin, cadmium (Cd) was the primary pollutant in cultivated soil in China. The continuous transport and accumulation of Cd in soil not only affects the soil ecological environment but also seriously threatens human health through the food chain, and other ways (Sun et al., 2021; Shen et al., 2016; Gong et al., 2021). Therefore, soil remediation and control of heavy metal pollution have always been the focus of soil environmental research. It is an economical, feasible, and effective method to control heavy metal pollution in soil by using improvers to adsorb and fix heavy metal elements and reduce heavy metal transport (Qiao et al., 2017; Yang T et al., 2022).

Iron-modified biochar, as an efficient and environmentally-friendly amendment has been widely used in soil remediation and control due to its advantages of low environmental risk, wide range of sources, and low price (Nguyen et al., 2023; Wan et al., 2020; Zhang et al., 2023; Jiao et al., 2022). Iron-modified biochar produced by high-temperature pyrolysis had developed pore structure and stable chemical properties. In addition, due to the complex reduction of Fe^{3+}, the surface functional groups of biochar increased, and the adsorption capacity of biochar for heavy metals was significantly improved (Zhou et al., 2018; Yang et al., 2021; Ryu et al., 2011; He et al., 2018). At present, there is increasing research on the adsorption capacity and mechanism of soil-heavy metals by modified biochar. For example, Zhou et al. (2022) studied the high removal of Cr^{6+} in iron-modified biochar/double-layer osmotic reaction barriers. Da et al. (2023) reported a decrease of Cd^{2+} availability in soil using K_2FeO_4-modified vinasse biochar due to the enrichment of surface functional groups. Li et al. (2022) demonstrated that the simultaneous immobilization mechanism of As^{3+}, Pb^{2+}, and Cd^{2+} with Mg-Al modified biochar/mining soil composites.

The solute transport model is an important means by which to study the transport process of heavy metals in soil and estimate the transport parameters accurately (Pei et al., 2021). With the deepening of the research on the transport process of heavy metals in soil, the research on the solute transport models have gradually attracted the attention of experts and scholars (Wang et al., 2020; Yuan et al., 2017; Yang et al., 2019; Jiang et al., 2019). Some researchers used chloridion (Cl^-) as a tracer ion and numerical models were used to predict the transport behavior of ions in the soil, such as copper, lead, zinc, and Cd (Pietrzak, 2021; Zhang et al., 2020b; Nguyen Ngoc et al., 2009). Anaman et al. (2022) used GIS and PMF methods found that the transport paths of As^{3+}, Cd^{2+}, Pb^{2+}, Cu^{2+}, and Zn^{2+} were mainly through surface runoff. Liu et al. (2022) found that the breakthrough curve (BTC) of Cd^{2+} was roughly of a slow 'S' type through simulation, and the simulated value of Cd^{2+} by the convection ediffusion equation (CDE) was close to the measured value. Zhou et al. (2009) found that BTC was accurately described by both the CDE equation and the two-zone model (TRM). However, the TRM model fitted the experimental data a little better than the CDE equation, which was possibly more convenient to use. In summary, there are increasingly more studies on the adsorption and transport of heavy metals in soil, but there are few studies on

the effect of iron-modified biochar on the transport of heavy metals in soil, and its transport model and parameters were especially unclear.

The objectives of this study were: (1) to investigate the effect of iron-modified biochar on the transport of Cl^- and Cd^{2+} in loessial soil by column experiments; and (2) to simulate the transport process and obtain relevant parameters of Cl^- and Cd^{2+} in loessial soil added iron-modified biochar using CDE equation and TRM model. The results could clarify the effects of different amounts of iron-modified biochar on heavy metals transport in loessial soil, and provide data reference for the prevention and treatment of heavy metal pollution in soil.

Materials and methods

Soil sample collection

The geographical location of the sampling point is Wangwa Town of Ningxia Province in China (106°37'20" ~ 106°39'25" E, 36°04'40" ~ 36°08'10" N), with an area of about 9.74 km^2. The terrain is complex, with crisscrossed terraces, beams, ridges, valleys, and gullies, and the elevation ranges from 1,698 to 1,903 m. It belongs to the semi-humid and semi-arid climate, with an average annual temperature of 7.1 °C, a daily temperature difference of 27 °C, and an average annual precipitation of about 400 mm. The spatial and temporal distribution of evaporation is uneven, mainly from July to September, and the average annual evaporation is about 1,000 mm. The main soil type is loessial soil, with clay contents of 8.78%, sand content of 17.88%, and silt content of 71.63%. The physical and chemical properties of loessial soil are shown in Table 1. The soil layer is deep and the soil is loose. The sampling depth was 0~10 cm, and five soil samples were obtained by the quince-shaped distribution method during sampling, which were fully mixed and then sampled by the quartering method. The collected soil samples were naturally air-dried and debris removed, and then ground and passed through a 2 mm soil sieve for use.

Preparation of iron-modified biochar

The woody biochar was purchased from Yixin Biotechnology Co. Ltd. (Table 1). Firstly, the woody biochar was pre-treated with mixed solution of $FeSO_4{\cdot}7H_2O$ and $Fe_2(SO_4)_3$ under vigorous stirring (800 mL deionized water was added to a 1 L beamer, then 5.0 g $FeSO_4{\cdot}7H_2O$ and 4.5 g $Fe_2(SO_4)_3$ were dissolved to obtain the mixed solution). After that, an even mixture was obtained by ultrasonic treatment for 1 h at 25 °C and was dried at 60 °C in a constant temperature oven. Finally, iron-modified biochar was obtained by pyrolysis in a Muffle furnace at 600 °C for 1 h. The as-prepared iron-modified biochar was ground and sieved for use (Gong et al., 2021). The physical and chemical properties of iron-modified biochar were shown in Table 2.

Solute transport test

The soil samples with different mass ratios of iron-modified biochar (0, 1%, 2%, 3%, 4%, and 5% as CK, T1, T2, T3, T4, and T5, respectively) were obtained by evenly mixing iron-modified biochar and soil (Liu et al., 2015). The solute transport experiments were conducted under plexiglass-columns (diameter of 5 cm and height of 20 cm, Fig. 1). The layer of filter paper was placed at the bottom of the plexiglass column to prevent the loading of uneven soil caused by soil particle leakage and blockage of the outflow hole. Each sample was filled in a plexiglass column with a thickness of 5 cm per layer and a total height of 15 cm. The roughening was trimmed between layers to make the soil of each layer fully contact and fill more evenly (the bulk weight of the soil sample: 1.43 $g{\cdot}cm^{-3}$). The upper and lower end of the soil column were a water supply outlet and a solution outlet composed of porous glass, respectively. The filter paper on the top soil surface of the soil column prevented the water supply from damaging the upper soil structure. In the test, a constant water head was maintained at 3 cm using a Markov bottle containing 0.1 $mg{\cdot}L^{-1}$ NaCl solution. When the soil column was completely saturated by NaCl solution, the water supply of the soil column was removed, and the surface water of the soil column was immediately sucked up. Then the NaCl solution was replaced with 15 $mg{\cdot}L^{-1}$ $Cd(NO_3)_2$ to remain water head at 3 cm (Liu et al., 2022). At the same time, a measuring cylinder of 25 mL was used to catch the leaching solution from the bottom end of the soil column, and the leaching solution was dumped once the cylinder was filled, and the time spent was recorded to calculate soil saturated hydraulic conductivity. The concentration of Cd^{2+} in the leaching solution was determined by ultraviolet spectrophotometry with Xylenol Orange disodium salt as a chromogenic agent and hexamethylenetetramine as buffer solution at 578 nm wavelength. The solute transport test was considered to be over when the differences of three consecutive Cd^{2+} concentrations were less than 1%. The solute transport parameters were calculated based on the experimental data. Finally, Cl^- content was determined by titration and Cd^{2+} content was determined by ultraviolet spectrophotometry.

Calculation of *Ks*

As one of the important soil hydraulics parameters, soil-saturated hydraulic conductivity (*Ks*, $cm{\cdot}min^{-1}$) refers to the water flux passing through saturated soil under a unit water potential gradient, which is a comprehensive reflection of soil texture, bulk density, pore distribution characteristics, and solute transport (Zhu et al., 2022). *Ks* can be calculated as Eqn (1):

$$Ks = Q \times L/A \times H \times t \quad (1)$$

where, *Q* (mL) and *L* (cm) are the flow rate and the height of soil column, respectively; *A* (cm^2), *H* (cm) and *t* (min) represent the cross-sectional area of the water flow, the total head difference of the seepage path and the transport time, respectively.

Solute transport model

BTC characterizes the relationship between the relative concentration of liquid flow and the change of pore volume (Mahapatra et al., 2023), which can reflect the characteristics of solute mixed displacement transport in soil (Pei et al., 2021). BTC is one of the important ways to investigate the mechanism of solute transport in soil. In this study, Cl^- and Cd^{2+} were used as the tracer ions to

Table 1. The physical and chemical properties of loessial soil.

Category	Organic matter ($g{\cdot}kg^{-1}$)	Total nitrogen ($g{\cdot}kg^{-1}$)	pH	Electrical conductivity ($uS{\cdot}cm^{-1}$)	Total potassium ($g{\cdot}kg^{-1}$)	Total phosphorus ($g{\cdot}kg^{-1}$)	Bulk density ($g{\cdot}cm^{-3}$)
Loessial soil	11.11	1.02	8.33	112.36	7.51	0.04	1.43

Table 2. The physical and chemical properties of iron-modified biochar.

Category	Total carbon (%)	Carbonization time (h)	Carbonization temperature (°C)	pH	Ash content	Pore size (> 2 mm)	Fe
Iron-modified biochar	55.63	1	600	7	22.86%	98.55%	23.02%

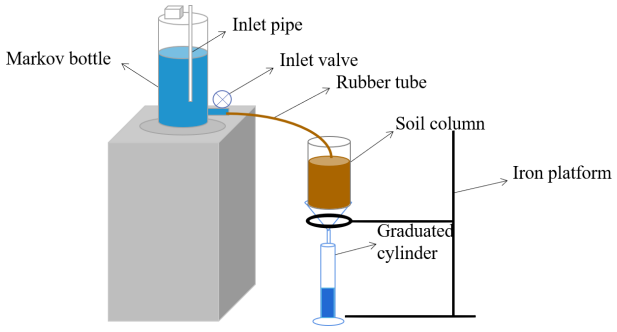

Fig. 1 Solute transport device.

investigate solute transport in saturated soil under one-dimensional steady water flow. The solute transport parameters were input into STANMOD software with the CXTFIT program nested.

The one-dimensional saturation CDE equation can be expressed as Eqn (2):

$$R\frac{\partial c}{\partial t} = D\frac{\partial^2 c}{\partial x^2} - V\frac{\partial c}{\partial x} \quad (2)$$

where, c (mg·L^{-1}) and t (h) are solute concentration and time, respectively; D (cm^2·h^{-1}) represents the dispersion coefficient, including diffusion and hydrodynamic dispersion; v (cm·h^{-1}), R and x (cm, x ≥ 0) stand for soil pore velocity, retardation coefficient and the distance of solute transport, respectively.

TRM model under the condition of steady flow can be described as Eqns (3)–(6):

$$\theta_m\frac{\partial C_m}{\partial t} + \theta_{im}\frac{\partial C_{im}}{\partial t} = \theta_m D\frac{\partial^2 C_m}{\partial x^2} - V_m\theta_m\frac{\partial C_m}{\partial x} \quad (3)$$

$$\theta_m\frac{\partial C_m}{\partial t} = \omega(C_m - C_{im}) \quad (4)$$

$$\theta = \theta_m + \theta_{im} \quad (5)$$

$$\beta = \theta_m/\theta \quad (6)$$

where, θ represents soil volumetric water content, cm^3·cm^{-3}; θ_m and θ_{im} represent the volumetric water content in the movable and immovable regions, respectively. C_m and C_{im} (μg·ml^{-1}) represent solute concentrations in mobile and immobile regions, respectively. Vm (cm·h^{-1}), ω (1 h^{-1}) and β represent the average pore velocity in the mobile zone; the mass exchange coefficient between the two zones and the ratio of water content in the mobile area, respectively. The dispersion capacity of the solute in the pore medium can be described by dispersion (λ), which is related to the average particle size and uniformity of the pore medium. Thus, λ can be calculated as Eqn. (7):

$$\lambda = \frac{D}{V} \quad (7)$$

where, D (cm^2·h^{-1}) and v (cm·h^{-1}) represent the hydrodynamic dispersion coefficient and average interstitial water velocity, respectively.

Data processing and analysis

The transport of Cl^- and Cd^{2+} in loessial soil by adding iron-modified biochar was simulated using CDE and TRM models with the aid of the CXTFIT program. Then the parameters (i.e., v, D, determination coefficient R^2 and root mean square error *RMSE*) were obtained. SPSS 22.0 software was used for difference analysis and statistical test.

Results and analysis

Characterization

The as-prepared iron-modified biochar was characterized by Fourier transform infrared spectroscopy (FT-IR) analysis. FT-IR spectra of biochar (BC), iron-modified biochar (FeBC) before and after reaction are shown in Fig. 2. The characteristic peaks of BC at 3,396 cm^{-1} corresponded to the stretching vibration of the OH group (Zhao et al., 2013). The presence of the Fe-O/OH group at 500~1,640 cm^{-1} indicated the successful loading of Fe on the surface of FeBC (Zhu et al., 2020; Gotić et al., 2007 ; Zhang et al., 2020c). The characteristic peak of FeBC at 1,533 cm^{-1} (C=O/C=C group) was weaker than that of BC (Zhang et al., 2009), suggesting that the loading of Fe was realized by reacting with the C=O functional groups on the BC surface (Xu et al., 2012).

Effect of iron-modified biochar on *Ks*

The *Ks* is essential for managing soil and groundwater recharge, promoting soil health, and evaluating soil improvement strategies (Hervé-Fernández et al., 2023). The changes of *Ks* under different addition amounts of iron-modified biochar are shown in Fig. 3. Compared to CK, *Ks* of T1, T2, T3, T4, and T5 decreased to 93.70%, 84.13%, 83.33%, 79.60%, and 66.67%, respectively, indicating that *Ks* significantly decreased with the increase of iron-modified biochar amounts from 0 to 50 g·kg^{-1} (p < 0.05). The results indicated iron-modified biochar was conducive to slowing down the transport of Cd^{2+} in soil, which significantly enhanced the water holding capacity of soil.

Transport process of Cl^-

Figure 4 shows the transport of Cl^- in loessial soil with different iron-modified biochar addition amount. All BTC curves showed the

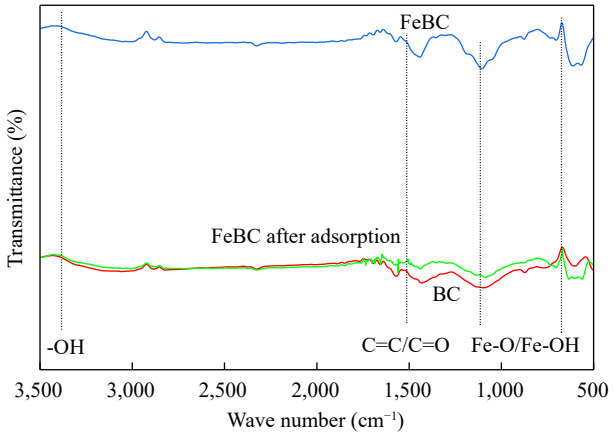

Fig. 2 FT-IR spectra of BC, FeBC, and FeBC after adsorption. BC represents biochar, FeBC represents iron-modified biochar without test, FeBC after adsorption represents iron-modified biochar adsorbed with heavy metals after test.

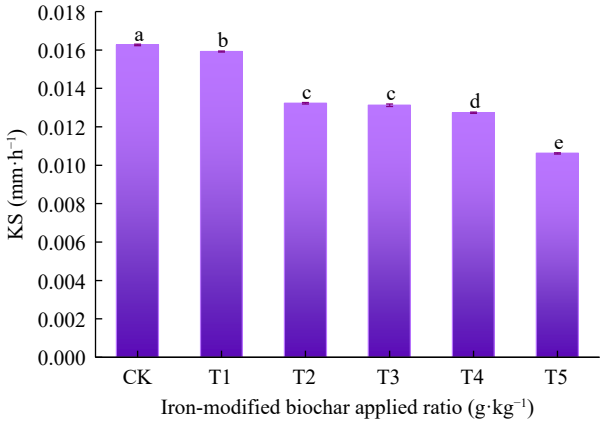

Fig. 3 The effect of iron-modified biochar on soil *Ks*. Different lowercase letters indicate significant difference between different treatments (p < 0.05).

S-like characteristics, which was consistent with the results of Zhou et al. (2009) studied on the BTC curve of Cl^-, but the shape and change trend under different iron-modified biochar contents were slightly different. BTC curves of Cl^- in loessial soil with iron-modified biochar showed that relative concentration gradually increased with the increasing time. Compared to CK, BTC curves of other treatments shifted to the right with increasing amounts of iron-modified biochar, and showed obvious trailing characteristics due to different amounts of iron-modified biochar added in loessial soil.

Initial penetration time (Te), complete penetration time (Ts), and total penetration time (Tt) are important characteristic parameters of solute penetration, which are jointly determined by pore water velocity and hydrodynamic dispersion coefficient of soil. Table 3 shows the the transport time of Cl^- in loessial soil with added iron-modified biochar. Te, Ts, and Tt were all positively correlated with the addition amounts of iron-modified biochar, indicating the longer transport process under the greater amount of iron-modified biochar. As listed in Table 3, Te of Cl^- increased from 8.57 to 12.76 h with the increasing application amounts of iron-modified biochar from 0 to 50 mg·kg^{-1}. Ts of Cl^- (exudate concentration equal to initial solution concentration) was also increased from 84.95 to 122.20 h, revealing that the time of complete migration equilibrium gradually extended with the increasing amounts of iron-modified biochar.

To further investigate the effect of iron-modified biochar on Cl^- transport in loessial soil, the transport curve of Cl^- in loessial soil by adding different iron-modified biochar was fitted using the CDE equation and TRM model. The main parameters of the CDE equation and TRM model are summarized in Table 4. The fitting effect of the TRM model was better than the CDE equation due to the higher R^2 more than 0.985 and lower (*RMSE*) less than 0.306. The values of the average pore water velocity (*v*) decreased with the increasing amounts of iron-modified biochar, indicating that adding of iron-modified biochar decreased the pore size of loessial soil and reduced the soil pore water velocity.

λ refers to the dispersion capacity of the solute in the pore medium (Dong et al., 2023), its size is related to the average particle size and uniformity of the pore medium, which is numerically equal to the ratio of hydrodynamic dispersion coefficient (*D*) and v, the greater the value, the stronger the diffusion capacity of the solute in the pore medium.

The values of λ for the CDE equation and the TRM model also increased with the increasing amounts of iron-modified biochar, which indicated the diffusion capacity of Cl^- was enhanced.

Transport process of Cd^{2+}

Figure 5 shows the change of the BTC curve of Cd^{2+} in loessial soil under different addition amounts of iron-modified biochar. Unlike the BTC curves of Cl^-, BTC curves of Cd^{2+} showed smooth L-like characteristics except for T4 and T5 treatments, and the concentration of Cd^{2+} in the effluent changed with time. The BTC curves of Cd^{2+} with different contents of iron-modified biochar in loessial soil showed that the concentration of Cd^{2+} increased gradually from low to high with time. Compared with CK, the BTC curves of Cd^{2+} with different addition amounts of iron-modified biochar all shifted to the right, and with the increase of iron-modified biochar, the BTC curve shifted to the right to a greater extent. The results showed that the addition of iron-modified biochar had a retarding effect on Cd^{2+} transport in loessial soil.

Table 5 showed the transport time of Cd^{2+} under different addition amounts of iron-modified biochar. It could be seen that Te, Ts, and Tt were all positively correlated with the addition amounts of iron-modified biochar, that was, the greater the application amount of-iron modified biochar, the longer the solute Te and Ts, and the longer the penetration process. The Te of Cd^{2+} under different addition amounts of iron modified biochar were 6.54, 6.70, 8.03, 9.86, 9.92, and 10.00 h, respectively.

It could be concluded that Te lengthened with the increase of iron modified biochar addition amounts. The Ts of Cd^{2+} reaching transport equilibrium (exudate concentration equal to initial solution concentration) in loessial soil with different amounts of iron-modified biochar were 80.67, 82.62, 95.16, 118.97, 119.39, and 124.94 h, respectively. It could be seen that with the increase of iron-modified biochar addition amounts, the time of Cd^{2+} transport

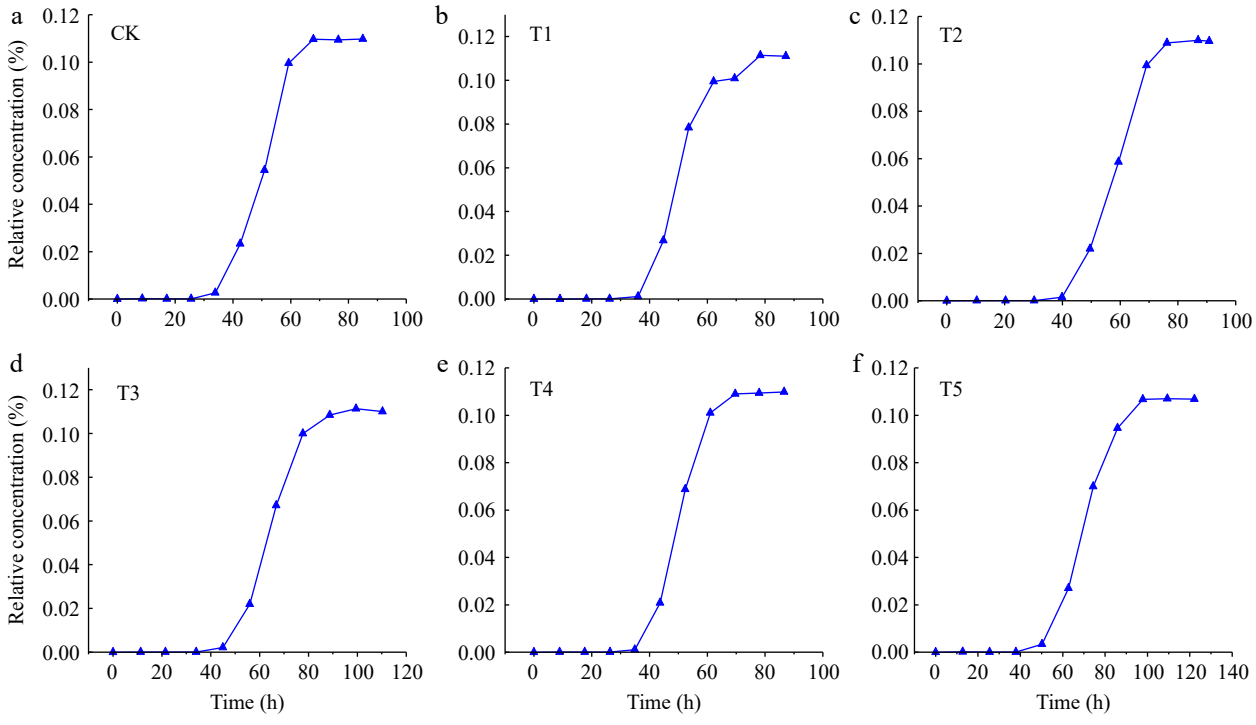

Fig. 4 The breakthrough curves of Cl^- in loessal soil with different iron-modified biochar contents.

Table 3. The transport time of Cl^- under different iron-modified biochar addition amounts.

Treatment	Te (h)	Ts (h)	Tt (h)
CK	8.57	84.95	76.38
T1	8.99	87.20	78.21
T2	10.35	98.82	88.47
T3	11.38	110.25	98.87
T4	12.16	115.59	77.75
T5	12.76	122.20	109.44

Te represents initial penetration time, Ts represents complete penetration time and Tt represents total penetration time.

Table 4. The relevant model parameters obtained by Cl^- transport curve fitting.

Parameters	Model name	CK	T1	T2	T3	T4	T5
v ($cm \cdot h^{-1}$)	CDE	0.376	0.329	0.264	0.227	0.201	0.135
	TRM	0.308	0.307	0.266	0.241	0.217	0.203
D ($cm^2 \cdot h^{-1}$)	CDE	0.100	0.100	0.100	0.100	0.100	0.224
	TRM	0.575	0.100	0.100	0.100	0.100	0.174
λ	CDE	0.266	0.304	0.379	0.441	0.498	0.741
	TRM	0.286	0.326	0.375	0.415	0.406	0.857
β	TRM	0.100	0.100	0.114	0.249	0.974	0.999
ω	TRM	0.100	0.100	0.557	0.596	0.786	0.851
R^2	CDE	0.887	0.944	0.906	0.929	0.938	0.927
	TRM	0.980	0.990	0.985	0.994	0.994	0.999
RMSE	CDE	0.326	0.364	0.272	0.249	0.235	0.201
	TRM	0.306	0.287	0.241	0.230	0.222	0.134

v represents average pore water velocity, D represents hydrodynamic dispersion coefficient, λ represents the dispersion capacity of the solute in the pore medium, β represents the percentage of solute in the total soil concentration and in the mobile region under equilibrium conditions, ω represents parameter of the degree of solute exchange between movable and immovable regions, R^2 represents coefficient of determination, *RMSE* represents the square root of the mean variance between the simulated value of the model and the measured value.

equilibrium was gradually extended, and the extent of the extension was increasing.

The applicability of different mathematical models to Cd^{2+} transport was compared and analyzed, and the main parameters of the CDE equation and TRM model were fitted in this paper (Table 6). From the results of parameter fitting, the R^2 was close to 1. The values of all v decreased with the increasing iron-modified biochar amounts, indicating that iron-modified biochar could reduce the velocity of soil pore water and effectively slow down the transport of Cd^{2+} in loessial soil. λ values of the CDE equation and TRM model were larger than CK. *RMSE* refers to the square root of the mean variance between the simulated value of the model and the measured value. The smaller the value of *RMSE* is, the closer the simulated value is to the measured value. The simulation results of both the CDE equation and the TRM model showed that the *RMSE* value of TRM was smaller than that of CDE, indicating that the simulated value of the TRM model was closer to the measured value and the fitting result was better.

To more intuitively analyze the difference and connection between measured values and simulated values, the breakthrough curves of Cd^{2+} under CK, 1%, 2%, 3%, 4%, and 5% treatments were simulated by the CDE equation and TRM model (Fig. 6). The simulation results from CK to T4 were shown, the fitting results from the CDE equation had different degrees of alienation from experimental data, whereas the fitting results from the TRM model were in good agreement with experimental data without the obvious estrangement, indicating that the solute transport process of Cd^{2+} could be better simulated by the TRM model compared to the CDE equation. The simulation results of the T5 treatment showed that both the CDE equation and the TRM model could fit well.

Discussion

Ks represents the ease with which water flows through soil when pore spaces are filled with water, which is an important hydraulic parameter used to investigate the transport characteristics of soil solute (Shwetha et al., 2015). *Ks* is closely related to soil physical properties such as soil bulk density and pore distribution (Jačka et al., 2018). Similar to the results of this study, Nakhli et al. (2021) observed biochar amendments decreased *Ks* of soil. Another study by Lim et al. (2018) observed *Ks* decreased when either larger or

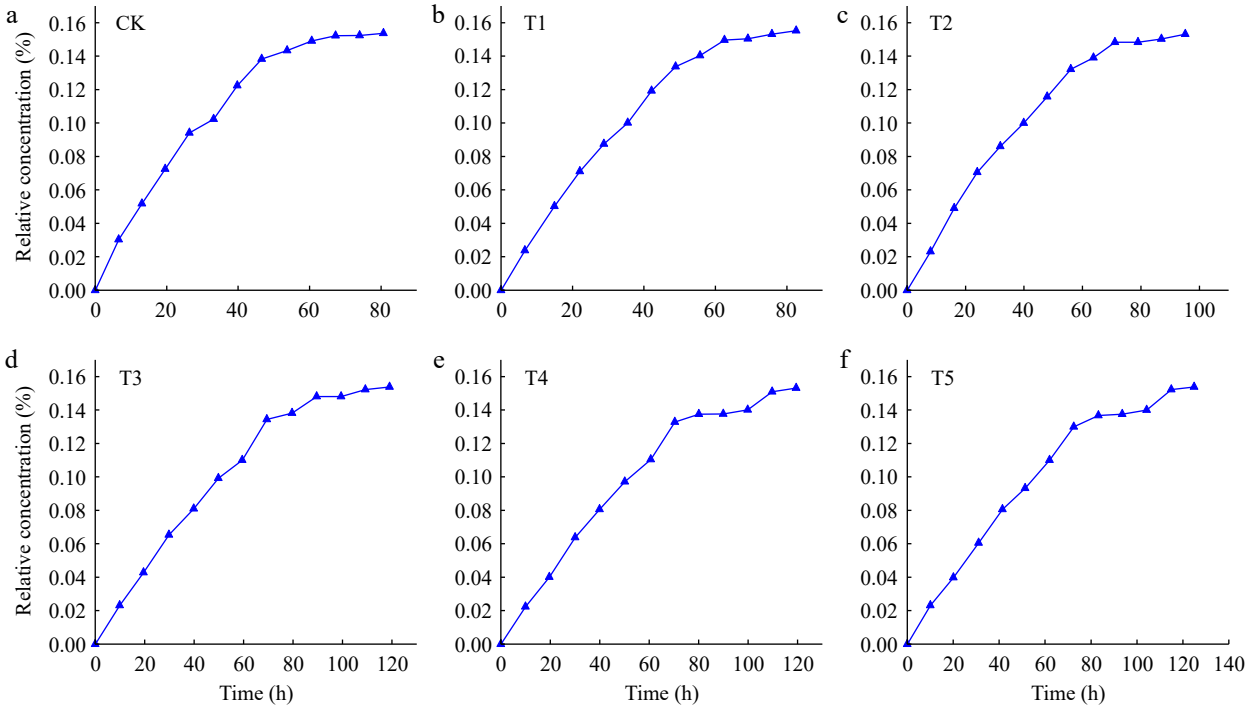

Fig. 5 Cd^{2+} breakthrough curves of iron-modified biochar in loessial soil.

Table 5. Transport time of Cd^{2+} under different iron-modified biochar amounts.

Treatment	Te (h)	Ts (h)	Tt (h)
CK	6.54	80.67	74.13
T1	6.70	82.62	75.92
T2	8.03	95.16	87.13
T3	9.86	118.97	109.11
T4	9.92	119.39	109.47
T5	10.00	124.94	114.94

Te represents initial penetration time, Ts represents complete penetration time, and Tt represents total penetration time.

smaller-size macadamia nutshell and pine chip biochar particles were added to the soil.

The transport equilibrium time of Cd^{2+} in loessial soil was significant delayed with the increasing iron-modified biochar amounts. The addition of iron-modified biochar increased the number of small pores in loessial soil, whereas the flow of water and the interconnected pores were decreased, which would lead to the complexity and uniformity of the pore structure of saturated soil. The soil pores with uneven size and distribution would cause different flow velocity, so an unbalanced solute front was formed in the soil profile, resulting in the extension of the transport time (Dong et al., 2023).

The BTC curve of Cd^{2+} in loessial soil was analyzed under different addition amounts of iron-modified biochar. As the BTC curve shifted to the right with the increase of the addition amounts of iron modified biochar, the penetration of Cd^{2+} in loessial soil was significantly delayed. The penetration time was significantly extended when the relative concentration reached the highest. This was consistent with the penetration results of Cd^{2+} transport in complex heavy metal contaminated sites by Liu et al. (2022). The results of the CDE equation and TRM model showed that *v* decreased with the increase of the amount of iron-modified biochar, indicating that the application of iron-modified biochar reduced the velocity of soil pore water and slowed down the transport of Cd^{2+} in loessial soil. The increase

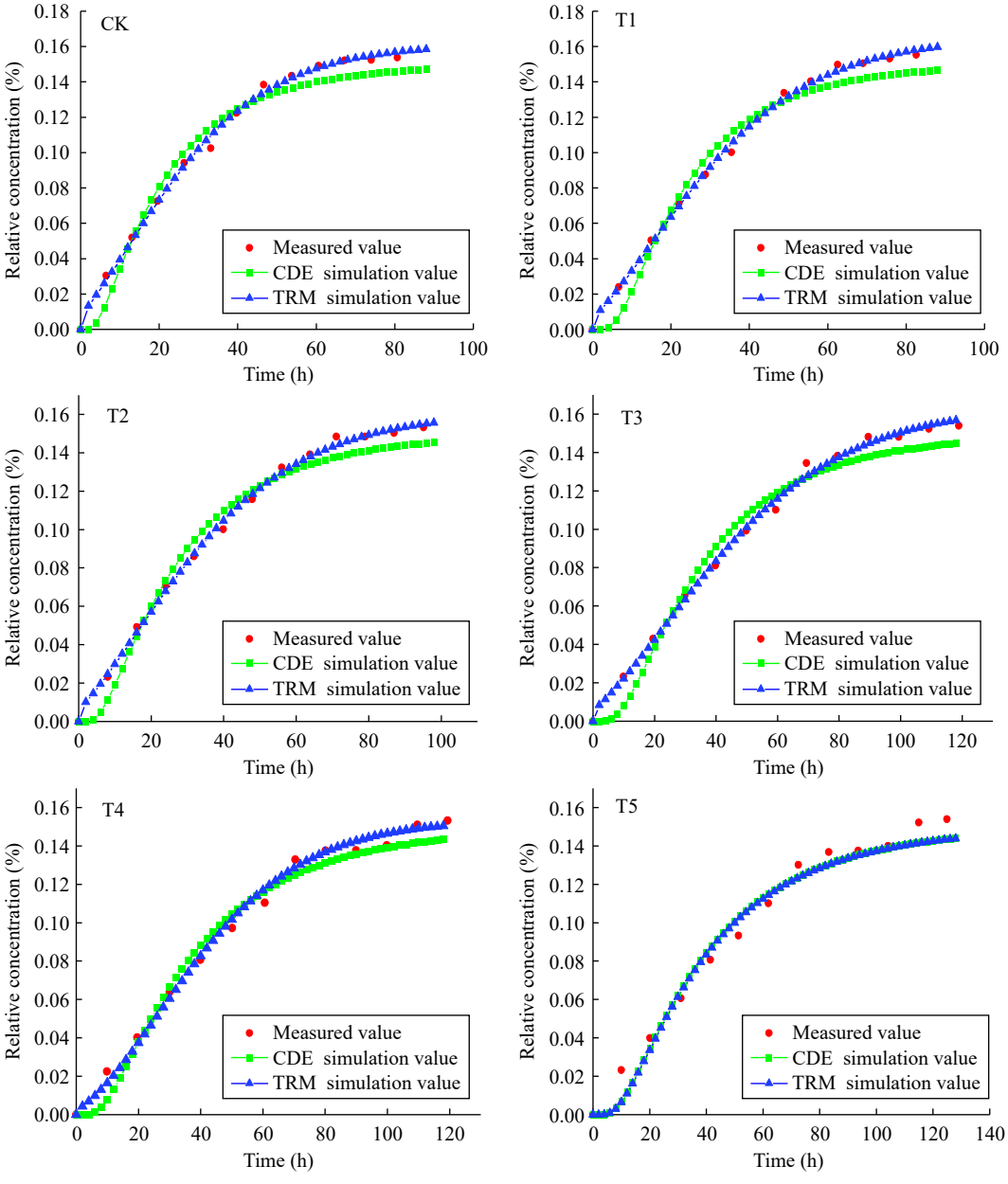

Fig. 6 Comparison of breakthrough curves of Cd^{2+} fitted by CDE and the TRM model.

Table 6. The relevant model parameters obtained by Cd^{2+} transport curve fitting.

Parameters	Model name	CK	T1	T2	T3	T4	T5
v ($cm \cdot h^{-1}$)	CDE	0.882	0.723	0.659	0.489	0.478	0.452
	TRM	0.557	0.476	0.433	0.384	0.354	0.307
D ($cm^2 \cdot h^{-1}$)	CDE	0.602	0.212	0.409	0.264	0.281	0.265
	TRM	0.140	0.120	0.108	0.118	0.274	0.220
λ	CDE	0.293	0.540	0.586	0.588	0.621	0.683
	TRM	0.251	0.252	0.249	0.307	0.717	0.774
β	TRM	0.100	0.100	0.100	0.100	0.248	0.845
ω	TRM	0.200	0.214	0.201	0.224	0.278	0.785
R^2	CDE	0.997	0.972	0.979	0.973	0.979	0.976
	TRM	0.997	0.998	0.998	0.996	0.993	0.976
RMSE	CDE	0.770	0.835	0.619	0.828	0.602	0.691
	TRM	0.114	0.781	0.580	0.134	0.246	0.350

v represents average pore water velocity, D represents hydrodynamic dispersion coefficient, λ represents the dispersion capacity of the solute in the pore medium, β represents the percentage of solute in the total soil concentration and in the mobile region under equilibrium conditions, ω represents parameter of the degree of solute exchange between movable and immovable regions, R^2 represents coefficient of determination, *RMSE* represents the square root of the mean variance between the simulated value of the model and the measured value.

of λ from the CDE equation and TRM model with the increasing amounts of iron-modified biochar could be caused by the addition of iron-modified biochar, which increased the pore complexity of loessial soil. The iron-modified biochar caused blockage of some pores, the curvature of the water channel and unconnected pore area increased, and the pore water flow rate decreased (Berkowitz et al., 2000). Therefore, iron-modified biochar slowed down and prevented the transport of Cd^{2+} in loessial soil. The adsorption capacity of iron-modified biochar to heavy metals increased significantly due to the increase of surface functional groups (Zhou et al., 2018). The β was the percentage of solute in the total soil concentration and the mobile region under equilibrium conditions (Satyawali et al., 2011; Schulin et al., 1987). the adsorption capacity of iron modified biochar to heavy metals increased significantly due to the increase of surface functional groups. According to fitting of TRM, the increase of β (from 0.100 to 0.845) indicated that the physical process of solute transport was more balanced with the increasing amounts of iron-modified biochar.

Although the Cd^{2+} transport process of loessial soil after the application of iron-modified biochar was studied and simulated in this paper, and the characteristics and rules of soil Cd^{2+} transport were analyzed, this paper mainly focused on the study and analysis of the influence mechanism of iron-modified biochar, which may have certain differences and limitations from the actual application in the field. In the future, this research group will conduct a more in-depth and systematic study on the transport process of heavy metals in soil through field experiments and long-term follow-up studies, so as to provide more reliable data support for the utilization of iron-modified biochar and the prevention and control of soil contaminated by heavy metals in loessial soil.

Conclusions

In the present study, the effect of iron-modified biochar on the transport of Cl^- and Cd^{2+} in loessial soil was investigated and then fitted using the CDE equation and TRM model.

(1) Compared to CK, *Ks* gradually decreased to 93.70%, 84.13%, 83.33%, 79.60%, and 66.67% with the increase of iron-modified biochar addition amounts from 1%, 2%, 3%, 4%, and 5%, respectively. The results indicated iron-modified biochar in soil could enhance the water holding capacity of soil.

(2) The total transport time of Cd^{2+} increased (from 1.79 to 40.81 h) with the increase of iron-modified biochar addition amounts, because the addition of iron-modified biochar decreased the flow of water and the interconnected pores, and extended the transport time of Cd^{2+}.

(3) Compared to CDE, the transport of Cd^{2+} in loessial soil with adding iron-modified biochar could be better simulated by TRM model due to the higher R^2 (> 0.97). According to the fitting of TRM model, the increasing amounts of iron-modified biochar slowed down and prevented the transport of Cd^{2+} in loessial soil. These findings were crucial for the application of iron-modified biochar in remediation of heavy metal-contaminated soil.

Author contributions

The authors confirm contribution to the paper as follows: writing - original draft prepration, software: Ma C; investigation: Ma C, Yuan C, Ma Y; supervision, writing - review & editing; visualization; funding acquisition: Bai Y, Wang Y. All authors reviewed the results and approved the final version of the manuscript.

Data availability

All data generated or analyzed during this study are included in this published article.

Acknowledgments

This study was funded by the Natural Science Foundation of Ningxia Hui Autonomous Region Project (2023AAC03046, 2023 AAC02018) and the National Natural Science Foundation of China (NSFC) (32360321) and the Key Research and Development of Ningxia Hui Autonomous Region Project (2021BEG02011).

Conflict of interest

The authors declare that they have no conflict of interest.

Dates

Received 21 May 2024; Revised 26 September 2024; Accepted 14 October 2024; Published online 18 November 2024

References

Anaman R, Peng C, Jiang Z, Liu X, Zhou Z, et al. 2022. Identifying sources and transport routes of heavy metals in soil with different land uses around a smelting site by GIS based PCA and PMF. *The Science of the Total Environment* 823:153759

Berkowitz B, Scher H, Silliman SE. 2000. Anomalous transport in laboratory-scale, heterogeneous porous media. *Water Resources Research* 36:149–58

Da Y, Xu M, Ma J, Gao P, Zhang X, et al. 2023. Remediation of cadmium contaminated soil using K_2FeO_4 modified vinasse biochar. *Ecotoxicology and Environmental Safety* 262:115171

Dong P, Yin M, Zhang Y, Chen K, Finkel M, et al. 2023. A Fractional-order dual-continuum model to capture non-Fickian solute transport in a regional-scale fractured aquifer. *Journal of Contaminant Hydrology* 258:104231

Gil C, Boluda R, Rodríguez Martín JA, Guzmán M, del Moral F, et al. 2018. Assessing soil contamination and temporal trends of heavy metal contents in greenhouses on semiarid land. *Land Degradation & Development* 29:3344–54

Gong H, Huang J, Ding Z, Chi J. 2021. A potential method using magnetically modified wheat straw biochars for soil Cd extraction. *Ecological Engineering* 166:106240

Gotić M, Musić S. 2007. Mössbauer, FT-IR and FE SEM investigation of iron oxides precipitated from $FeSO_4$ solutions. *Journal of Molecular Structure* 834–836:445–53

He R, Peng Z, Lyu H, Huang H, Nan Q, et al. 2018. Synthesis and characterization of an iron-impregnated biochar for aqueous arsenic removal. *The Science of the Total Environment* 612:1177–86

Hervé-Fernández P, Muñoz-Arriagada R, Glucevic-Almonacid C, Bahamonde-Vidal L, Radic-Schilling S. 2023. Influence of rangeland land cover on infiltration rates, field-saturated hydraulic conductivity, and soil water repellency in southern *Patagonia*. *Rangeland Ecology & Management* 90:92–100

Jačka L, Trakal L, Ouředníček P, Pohořelý M, Šípek V. 2018. Biochar presence in soil significantly decreased saturated hydraulic conductivity due to swelling. *Soil and Tillage Research* 184:181–85

Jiang Y, Yin X, Guan D, Jing T, Sun H, et al. 2019. Co-transport of Pb(II) and oxygen-content-controllable graphene oxide from electron-beam-irradiated graphite in saturated porous media. *Journal of Hazardous Materials* 375:297–304

Jiao Y, Wang T, He M, Liu X, Lin C, et al. 2022. Simultaneous stabilization of Sb and As co-contaminated soil by Fe–Mg modified biochar. *The Science of the Total Environment* 830:154831

Li Q, Liang W, Liu F, Wang G, Wan J, et al. 2022. Simultaneous immobilization of arsenic, lead and cadmium by magnesium-aluminum modified biochar in mining soil. *Journal of Environmental Management* 310:114792

Lim TJ, Spokas K. 2018. Impact of biochar particle shape and size on saturated hydraulic properties of soil. *Korean Journal of Environmental Agriculture* 37:1–8

Liu X, Guo H, Zhang X, Zhang S, Cao X, et al. 2022. Modeling the transport behavior of Pb(II), Ni(II) and Cd(II) in the complex heavy metal pollution site under the influence of coexisting ions. *Process Safety and Environmental Protection* 162:211–18

Liu Y, Zhou B, Wang Q, Tan S. 2015. Effects of nano-carbon on water movement and solute migration characteristics of loessial soil. *Journal of Soil and Water Conservation* 29(1):21–25

Mahapatra U, Manna AK, Chatterjee A. 2023. Modeling of breakthrough curves in removal of Cr(VI) and methylene blue using immobilized activated carbon from natural rubber waste. *Bioresource Technology Reports* 24:101600

Muhammad H, Wei T, Cao G, Yu S, Ren X, et al. 2021. Study of soil microorganisms modified wheat straw and biochar for reducing cadmium leaching potential and bioavailability. *Chemosphere* 273:129644

Nakhli SAA, Goy S, Manahiloh KN, Imhoff PT. 2021. Spatial heterogeneity of biochar (segregation) in biochar-amended media: an overlooked phenomenon, and its impact on saturated hydraulic conductivity. *Journal of Environmental Management* 279:111588

Nguyen Ngoc M, Dultz S, Kasbohm J. 2009. Simulation of retention and transport of copper, lead and zinc in a paddy soil of the Red River Delta, Vietnam. *Agriculture, Ecosystems & Environment* 129:8–16

Nguyen TB, Sherpa K, Bui XT, Nguyen VT, Vo TDH, et al. 2023. Biochar for soil remediation: a comprehensive review of current research on pollutant removal. *Environmental Pollution* 337:122571

Pei Y, Huang L, Li D, Shao M. 2021. Characteristics and controls of solute transport under different conditions of soil texture and vegetation type in the water-wind erosion crisscross region of China's Loess Plateau. *Chemosphere* 273:129651

Pietrzak D. 2021. Modeling migration of organic pollutants in groundwater—review of available software. *Environmental Modelling & Software* 144:105145

Qiao J, Sun H, Luo X, Zhang W, Mathews S, et al. 2017. EDTA-assisted leaching of Pb and Cd from contaminated soil. *Chemosphere* 167:422–28

Ryu BG, Park GY, Yang JW, Baek K. 2011. Electrolyte conditioning for electrokinetic remediation of As, Cu, and Pb-contaminated soil. *Separation and Purification Technology* 79:170–76

Satyawali Y, Seuntjens P, Van Roy S, Joris I, Vangeel S, et al. 2011. The addition of organic carbon and nitrate affects reactive transport of heavy metals in sandy aquifers. *Journal of Contaminant Hydrology* 123:83–93

Schulin R, van Genuchten MT, Flühler H, Ferlin P. 1987. An experimental study of solute transport in a stony field soil. *Water Resources Research* 23:1785–94

Shen X, Huang DY, Ren XF, Zhu HH, Wang S, et al. 2016. Phytoavailability of Cd and Pb in crop straw biochar-amended soil is related to the heavy metal content of both biochar and soil. *Journal of Environmental Management* 168:245–51

Shwetha P, Varija K. 2015. Soil water retention curve from saturated hydraulic conductivity for sandy loam and loamy sand textured soils. *Aquatic Procedia* 4:1142–49

Sun T, Xu Y, Sun Y, Wang L, Liang X, et al. 2021. Cd immobilization and soil quality under Fe-modified biochar in weakly alkaline soil. *Chemosphere* 280:130606

Wan X, Li C, Parikh SJ. 2020. Simultaneous removal of arsenic, cadmium, and lead from soil by iron-modified magnetic biochar. *Environmental Pollution* 261:114157

Wang H, Liu J, Yao J, He Q, Ma J, et al. 2020. Transport of Tl(I) in water-saturated porous media: role of carbonate, phosphate and macromolecular organic matter. *Water Research* 186:116325

Xu T, Lou L, Luo L, Cao R, Duan D, et al. 2012. Effect of bamboo biochar on pentachlorophenol leachability and bioavailability in agricultural soil. *The Science of the Total Environment* 414:727–31

Yang J, Ge M, Jin Q, Chen Z, Guo Z. 2019. Co-transport of U(VI), humic acid and colloidal gibbsite in water-saturated porous media. *Chemosphere* 231:405–14

Yang T, Xu Y, Huang Q, Sun Y, Liang X, et al. 2021. An efficient biochar synthesized by iron-zinc modified corn straw for simultaneously immobilization Cd in acidic and alkaline soils. *Environmental Pollution* 291:118129

Yang T, Xu Y, Huang Q, Sun Y, Liang X, et al. 2022. Removal mechanisms of Cd from water and soil using Fe-Mn oxides modified biochar. *Environmental Research* 212:113406

Yuan Y, Peng X. 2017. Fullerol-facilitated transport of copper ions in water-saturated porous media: influencing factors and mechanism. *Journal of Hazardous Materials* 340:96–103

Zhang G, Liu H, Liu R, Qu J. 2009. Adsorption behavior and mechanism of arsenate at Fe-Mn binary oxide/water interface. *Journal of Hazardous Materials* 168:820–25

Zhang G, Liu X, Gao M, Song Z. 2020a. Effect of Fe-Mn-Ce modified biochar composite on microbial diversity and properties of arsenic-contaminated paddy soils. *Chemosphere* 250:126249

Zhang H, Lu T, Shang Z, Li Y, He J, et al. 2020b. Transport of Cd^{2+} through saturated porous media: insight into the effects of low-molecular-weight organic acids. *Water Research* 168:115182

Zhang JY, Zhou H, Gu JF, Huang F, Yang WJ, et al. 2020c. Effects of nano-Fe_3O_4-modified biochar on iron plaque formation and Cd accumulation in rice (*Oryza sativa* L.). *Environmental Pollution* 260:113970

Zhang K, Yi Y, Fang Z. 2023. Remediation of cadmium or arsenic contaminated water and soil by modified biochar: a review. *Chemosphere* 311:136914

Zhao L, Cao X, Mašek O, Zimmerman A. 2013. Heterogeneity of biochar properties as a function of feedstock sources and production temperatures. *Journal of Hazardous Materials* 256–257:1–9

Zhou B, Shao M, Shao H. 2009. Effects of rock fragments on water movement and solute transport in a Loess Plateau soil. *Comptes Rendus Géoscience* 341:462–72

Zhou Q, Lin L, Qiu W, Song Z, Liao B. 2018. Supplementation with ferromanganese oxide–impregnated biochar composite reduces cadmium uptake by indica rice (*Oryza sativa* L.). *Journal of Cleaner Production* 184:1052–59

Zhou Z, Liu P, Wang S, Finfrock YZ, Ye Z, et al. 2022. Iron-modified biochar-based bilayer permeable reactive barrier for Cr(VI) removal. *Journal of Hazardous Materials* 439:129636

Zhu K, Bin Q, Shen Y, Huang J, He D, et al. 2020. *In-situ* formed N-doped bamboo-like carbon nanotubes encapsulated with Fe nanoparticles supported by biochar as highly efficient catalyst for activation of persulfate (PS) toward degradation of organic pollutants. *Chemical Engineering Journal* 402:126090

Zhu P, Zhang G, Zhang B. 2022. Soil saturated hydraulic conductivity of typical revegetated plants on steep gully slopes of Chinese Loess Plateau. *Geoderma* 412:115717